Contents lists available at ScienceDirect

Polyhedron

journal homepage: www.elsevier.com/locate/poly

NMR investigations on a series of diplatinum (II) complexes possessing phenylpropenoids in $CDCl_3$ and CD_3CN: Crystal structure of a mononuclear platinum complex

Pham Van Thong [a], Nguyen Thi Thanh Chi [a,*], Mohammad Azam [b,*], Cu Hong Hanh [a], Le Thi Hong Hai [a], Le Thi Duyen [c], Mahboob Alam [d], Saud I. Al-Resayes [b], Nguyen Van Hai [a]

[a] Faculty of Chemistry, Hanoi National University of Education, 136 Xuan Thuy, Cau Giay, Hanoi, Vietnam
[b] Department of Chemistry, College of Sciences, King Saud University, PO BOX 2455, Riyadh 11451, Saudi Arabia
[c] Department of Chemistry, Faculty of Basic Science, Hanoi University of Mining and Geology, 18 Vien Street Duc Thang, Bac Tu Liem, Hanoi, Vietnam
[d] Division of Chemistry and Biotechnology, Dongguk University, Gyeongju 780724, Republic of Korea

ARTICLE INFO

Keywords:
Dinuclear Pt(II) complexes
Mononuclear Pt(II) complex
Arylolefin
Crystal structure
NMR spectroscopy

ABSTRACT

The NMR spectra of five diplatinum(II) complexes, Pt(μ-Cl)(arylolefin)]$_2$ [arylolefin = Eug (**1**), ^{i}PrEug (**2**), Meug (**3**), EtEug (**4**), Saf (**5**)], in $CDCl_3$ are studied. All the five complexes are formed by the reaction of K[$PtCl_3$(arylolefinH)] with Ag_2O in the mixture of alcohol-water. A mononuclear platinum complex, PtCl(Saf)(CH_3CN)], which is formed by the crystallization of a dimeric complex **5** in acetonitrile is also investiated. The mononuclear platinum complex is characterized by elemental analysis, ESI mass spectrometry, infrared and NMR spectroscopic studies and single crystal X-ray crystallography. The single X-ray crystal structure reveals the coordination of Pt(II) ion to Saf via C = C_{allyl} and the carbon of the benzene ring. DFT calculations are also performed to collect information about the structural parameter and stability of mononuclear platinum complexes. The findings reveal that the theoretical data agree with the experimental findings of single crystal X-ray structure. In addition, Hirshfeld surface analysis is also carried out to investigate various intermolecular interactions in the crystal structure of mononuclear platinum complex.

1. Introduction

Platinum-based compounds have been extensively investigated as potential chemotherapeutic medicines since the revolutionary discovery of cisplatin and its analogs [1–3]. Despite their remarkable efficacy against various cancers, platinum-based drugs are accompanied by several serious adverse effects [4,5]. This motivates the scientists to see out more effective platinum complexes. Lippard et al discovered a novel platinum complex, cis-[$Pt(NH_3)_2$(Phenanthridine)Cl]NO_3, which is 7–40 times more effective than cisplatin in the early scan of human cancer cells from a range of organs [6].

The strategy of using a natural compound as a ligand in the formation of Pt(II) complexes to minimize their toxicity and consequently harmful consequences has gained a lot of interest in recent years [7–9]. The platinum complex K[$PtCl_3(C_2H_4)$], also known as Zeise's salt, was discovered by William Zeise in 1825 as the first example of a transition metal–olefin complex through the interaction of platinum chloride with ethylene [10]. Olefin ligands, also known as alkene ligands, are good π electron donors and are widely used in the organometallic chemistry of platinum to produce relatively stable complexes [10–13]. Pt(II) complexes with a single geometry and stability are useful models for bonding, structural, and reactivity research [14]. Over the years, several Pt(II) complexes with natural arylolefins as ligands, such as safrole (in sassafras oil), eugenol (in clove oil), and anethole (in anise and fennel oil), and their derivatives have been investigated due to their novel topologies and significant inhibitory activities against human cancer cells, and have shown significant anti-inflammatory and analgesic properties [9,15–17]. In addition, large number of Pt(II) complexes with caffeine [18], theophylline [19], methyleugenol [20,21], safrole [15,16], oleanoic acid [22], propyl gallate [23] have been synthesized and their biological applications explored. Moreover, several diplatinum(II) complexes (Scheme 1) containing phenylpropenoids, [Pt(μ-Cl)(arylolefin)]$_2$ have been reported in mild conditions [16,24–26], which, when combined with other ligands, L, yield monoplatinum(II) complexes with

* Corresponding author.
E-mail addresses: chintt@hnue.edu.vn (N.T.T. Chi), mhashim@ksu.edu.sa, azam_res@yahoo.com (M. Azam).

https://doi.org/10.1016/j.poly.2021.115612
Received 11 October 2021; Accepted 27 November 2021

the general formula [PtCl(arylolefin)(L)] (L: amine or *N*-heterocyclic carbene) [24,26–28]. However, some monoplatinum complexes have shown considerable anticancer properties [26,28]. Furthermore, the role of these complexes in catalysis has also been studied [27]. Despite the significant literature [9,15–17], the structure of these dimeric complexes has yet to be thoroughly investigated.

Herein, in this article, we will investigate the NMR studies of five diplatinum complexes [Pt(μ -Cl)(arylolefin)]$_2$ (**1–5**) in $CDCl_3$ and CD_3CN. In addition, a mononuclear platinum complex, [PtCl(Saf)(CH_3CN)] obtained from the slow evaporation of the diplatinum complex **5** upon recrystallization in acetonitrile at room temperture will also be investigated. However, the mononuclear platinum complex [PtCl(Saf)(CH_3CN)] has been characterized by elemental analyses, FT-IR, ESI-MS, NMR spectroscopic studies and single crystal X-ray crystallography. Time-dependent NMR spectroscopy has attracted lot of attention as it is used to better understand the synthesis of platinum complexes [29]. As the name suggests, time-dependent is used in NMR spectroscopic approach to improve the intensity and resolution of a group of peaks over time, allowing for a more precise interpretation of chemical structure of platinum complex. Therefore, Time-dependent DFT studies are also carried out to to know about the bonding insights into the structure of monoplatinum complex using B3LYP-6-31G(d,p)/LANL2DZ level of theory [30]. In addition, Hirshfeld surface analysis is also performed to determine various intermolecular interactions in the crystal structure of mononuclear platinum complex.

2. Experimental

2.1. Materials and methods

All chemicals and solvents (AR grade) used in the experiment were obtained from Sigma and used as received. The NMR spectra of complexes **1**–**4** was recorded on Bruker AVANCE 500 MHz with TMS as an internal standard in chloroform-d_1 and acetonitrile-d_3. However, NMR spectra for complex **5** were recorded on Bruker AVANCE 300 MHz with TMS as an internal standard in acetonitrile-d_3. The elemental analysis for complex [PtCl(Saf)(CH_3CN)] was performed on a Perkin-Elmer PE 2400 elemental analyzer. The ESI-Mass spectrum was measured using a Finnigan MAT LCQ spectrometer. Infrared spectra were recorded on IMPACK-410 NICOLET spectrometer as KBr discs in the range 400–4000 cm^{-1}. The single crystal X-ray diffraction was carried out on a Bruker AXS SMART APEX diffractometer using graphite monochromatic MoKα radiation (λ = 0.71073 Å). The software packages SMART [31], SAINT [32], SHADABS [33] and SHELXTL [34] were used for data collection, reflection indexing, determination of lattice parameters, integration of reflections and scaling, empirical absorption correction, space group determination, structure solution, and refinements, respectively. Anisotropic thermal parameters were refined for the remaining non-hydrogen atoms. The hydrogen atoms were placed in their ideal positions.

2.2. Synthesis of complexes *1–5*

The complex [Pt(μ-Cl)(Eug)]$_2$ (**1**) was synthesized in high yield following the protocols described in the literatures [26]. However, when Ag_2O was used instead of $AgNO_3$ in the synthetic procedure, the yield of complex **1** increased from 40 % to 65 %. A mixture of Ag_2O (278 mg, 1.2 mmol) and K[$PtCl_3$(EugH)] (505 mg, 1.0 mmol,) in an ethanol–water mixture (12 mL, 1:5, *v/v*) in round bottom flask covered with aluminum foil to shield from light was stirred at room temperatue for 6 h. The reaction mixture was extracted with chloroform multiple times until the chloroform phase became colorless. The solvent from the resultant organic phase was removed under vacuum, yielding a solid product, which was washed with acetone and dried under vacuum. The product was recrystallized in chloroform, providing lemon yellow small crystals suitbale for single crystal X-ray diffraction. Complexes [Pt(μ-Cl)(arylolefin)]$_2$ ((arylolefin: ^{i}PrEug/**2** [25], Meug/**3** [24], EtEug/**4** [24], Saf/**5** [16]) were synthesized using the precursor K[$PtCl_3$(arylolefin)] as described previously with yield 70%, 80%, 65% and 75% , respectively. The synthesized complexes yielded lemon yellow crystals upon crystallization in chloroform. However, complex **5** on recrystallization in concentrated acetonitrile solution provides crystals on slow evaporation at room temperature over 24 h for mononuclear platinum complex, [PtCl(Saf)(CH_3CN)]. The crystals were found appropriate for single crystal X-ray diffraction.

Anal. Calc. for $C_{12}H_{12}O_2NClPt$: C, 33.29; H, 2.77; N, 3.24. Found: C,

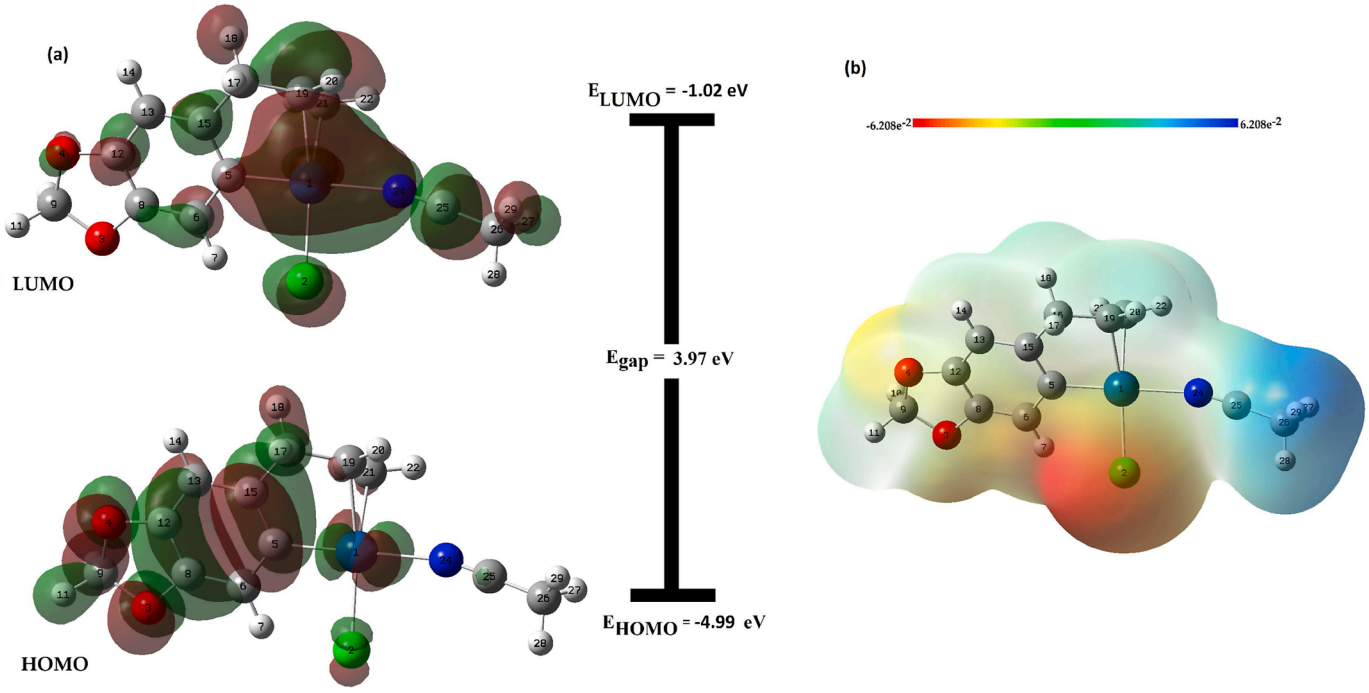

Scheme 1. *Anti*-structure of complexes **1**–**5** and the ligands (the numeration on structures used for NMR analysis).

33.27; H, 2.60; N, 3.23. -MS (ESI) Calcd for [M − CH_3CN + Cl]$^-$, $C_{10}H_9O_2Cl_2Pt$: *m/z* 427. Found (%): *m/z* 427 (100). Calcd for [2 M − $2CH_3CN$ + Cl]$^-$, $C_{20}H_{18}O_4Cl_3Pt$: *m/z* 819. Found (%): *m/z* 819 (60). FT-IR (KBr pellet, cm^{-1}): 2302 (CN); 1602, 1507, 1460 (C═C).

2.3. Theoretical investigations

The Gaussian 09 program package [35] was used to perform quantum chemical calculations on the X-ray structure of mononuclear platinum complex, [PtCl(Saf)(CH_3CN)]. The crystallographic information file (cif) of the complex was used as an input file for theoretical calculations with GaussView [36], which was also used for post-processing in the result description. The ground state geometries of the complex were optimized in the gas phase using Becke's three-parameter Lee-Yang-Parr (B3LYP) DFT functional with 6-31G(d,p) basis set for Cl, O, H, N, C atoms and LANL2DZ for Pt atoms for FMOs and MEP studies. Crystal Explorer (21.5 v) [37] was used to calculate Hirshfeld surfaces and corresponding 2D fingerprint plots over the crystal structure of [PtCl(Saf)(CH_3CN)].

3. Results and discussion

The complexes [Pt(μ-Cl)(arylolefin)]$_2$ (**2**–**5**) were synthesized in high yield (65–80%) using the procedure reported in the literatures [16,24,25]. However, the synthesis of complex [Pt(μ-Cl)(Eug)]$_2$ (**1**) was improved by utilizing Ag_2O instead of $AgNO_3$, resulting in the higher yield of 65 %, from 40% [26].

Complexes **1**–**5** are insoluble in water, ethanol, and acetone, but soluble in chloroform and acetonitrile. However, complex **5** is not soluble in chloroform. Complexes **1**–**4** have lemon-yellow color in chloroform, but look light yellow in acetonitrile.

Complexes **1**–**5** with *anti*-structures as proposed in Scheme 1 were reported in previous investigations using ESI MS, IR and NMR spectral analyses [16,24–26]. The occurrence of two sets of signals in the ^{1}H NMR spectra of **1**–**4** in $CDCl_3$ has, however, not yet been discussed [Supplementary Information Figs. S1, S3, S4, S5, S6]. Furthermore, several analogs of complexes **1**–**5**, such as [PtCl(μ-Cl)(alkene)]$_2$ [38], [PtCl(μ-Cl)(alkyne)]$_2$ [38], [Pt(μ-Cl)(κ^2-*P,C*)]$_2$ [39] and [Pt(μ-Cl)(κ^2-*N, C*)]$_2$ [40] exist in both *anti* and *syn* isomers. The time-dependent ^{1}H NMR spectra of [Pt(μ-Cl)(Eug)]2 **1** in $CDCl_3$ were studied to see if the complex has similar structural properties [Supplementary Information Fig. S2] [26]. Complex **5** is insoluble in $CDCl_3$, which prevents us from participating in the same study. Furthermore, while trying to develop single crystals of complex **2** in acetonitrile, we discovered a mononuclear complex [PtCl(^{i}PrEug)(CH_3CN)] by serendipity [41]. In this investigation, we additionally studied the ^{1}H and ^{13}C NMR spectra of complexes **3**–**5** in CD_3CN [Supplementary Information Figs. S7, S8, S9, S13, S14]. The chemical shift (δ), intensity, shape, spin–spin splitting pattern were used to assign the ^{1}H and ^{13}C signals in the spectra. The ambiguous ^{1}H and ^{13}C signals were additionally assigned using the HSQC, HMBC and NOESY spectra [Supplementary Information Figs. S10, S11, S12]. The signal at 123.0 ppm, for example, has cross peak A of H3 and cross peak B of H8a, indicating that it belongs to C5 (Fig. 1). The signal at 142.0 ppm, belonging to C4 is confirmed by the cross-peak C of H6 and cross peak D of H9. The signal of C1 at 146.0 ppm was confirmed on the basis of cross peak E with H3. The cross-peak F of the signal at 6.55 ppm with two ^{195}Pt satellites of H6 indicate the signal at 148.8 for *C*2. The assigned ^{1}H and ^{13}C NMR signals are listed in Table 1 and Table 2, respectively. Figs. 2 and 3 show the time-dependent ^{1}H NMR spectra of **2** in $CDCl_3$ and the ^{13}C NMR spectra of **3** in $CDCl_3$ and CD_3CN, respectively.

Table 1 shows that the ^{1}H NMR spectra of **1**–**4** in $CDCl_3$ have certain similar properties. Firstly, two sets of signals in 1:1 ratio are observed, and they don't change throughout the course of 48 h (Fig. 2). There are only a few signals that differ slightly (bold highlight in Table 2). The proton H6, for example, produces two singlets at 6.41 and 6.38 ppm for

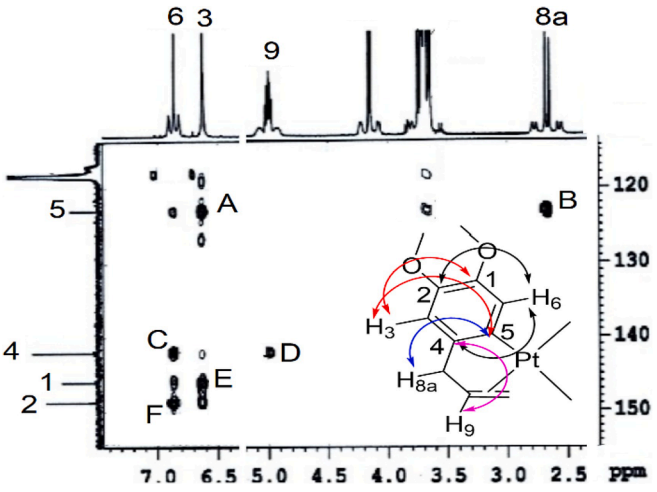

Fig. 1. Partial HMBC NMR spectrum of **3** in CD_3CN.

2, 6.47 and 6.46 ppm for 3, and 6.43 and 6.46 ppm for **4**. Second, strong evidence in both sets of signal was found to support the coordination of arylolefin with Pt(II) *via* C = C_{allyl} and C5 of benzene ring: i) all H9, *H*10 resonances shift upfield in comparison to non-coordinated arylolefin [16,24–26]; ii) only two singlets are observed for H3 and H6 at 6.53–6.69 in the spectra of the free arylolefin. However, no signal was observed for H5; iii) The ^{195}Pt satellites from the signals of H9, *H*10, H8 are clearly observed with the distance between them ($^2J_{PtH}$ for H9 and *H*10, 65–75 Hz, $^3J_{PtH}$ for H8, 105–110 Hz) (Table 1). In light of the foregoing observations, it can be concluded that complexes **1**–**4** exist in two isomers with *syn* and *anti*-structures in both solid-state and chloroform solution, as reported in Scheme 2. However, both these isomers in the investigated condition are not interchangeable. This is corroborated by the findings in the ^{13}C NMR spectra of **2** and **3** in $CDCl_3$ (Table 1 and Fig. 3a). In particular, two sets of signals arise in each spectrum that is characteristic of the coordination of aryolefins with Pt(II) as π/σ-chelator ligands [27]. Although there are no ^{1}H NMR spectra of **5** in $CDCl_3$, the existence of **1**–**4** in solid form can be utilized to demonstrate the presence of analog **5**.

A question has been raised over whether complexes **1**–**5** in CD_3CN also have the two syn/anti isomers or give complexes of the type [PtCl(arylolefin)(CH_3CN)] as complex **2** did. Therefore, to answer this question, the ^{1}H and ^{13}C NMR spectra of **3**–**5** in CD_3CN were explored. The assigned results in Table 2 reveal that each spectrum has only a single set of signals that differs from the equivalent spectrum recorded in $CDCl_3$, suggesting that the two syn/anti isomers of **3**–**5** were transformed to different complexes in CD_3CN. Furthermore, the NMR signals of the arylolefins H9, *H*10, C9, C10, H3, and H6 in Table 2 reveal that they are coordinated with Pt(II) as π/σ-chelator ligands, as observed in $CDCl_3$. These results can be explained due to the cleavage of the bridge chlorido in the dimeric complexes **3**–**5** by coordinating solvent CD_3CN to form mononuclear complexes of general formula [PtCl(arylolefin)(CH_3CN)]. Elemental analysis, ESI mass spectrometry, IR, and XRD methods were used to identify the structure of the [PtCl(Saf)(CH_3CN)] complex.

The ESI mass spectra of [PtCl(Saf)(CH_3CN)] in the negative mode reveals the existence of a base peak with a relative intensity of 100%, which is consistent with pseudomolecular anion [$PtCl_2$(Saf)]$^-$, suggesting the coordination of Saf and CH_3CN. Furthermore, the calculated pattern on the basis of zoom scan spectrum corresponds to the isotopic envelopes of the anion [Figs. 4, 5].

The IR spectra of [PtCl(Saf)(CH_3CN)] exhibits bands for the coordination of Saf and CH_3CN. The existence of CH_3CN in the complex is shown by the weak absorption band for $\nu_{C\equiv N}$ at 2302 cm^{-1}. However, decrease in frequency of the characteristic band for the $\nu_{C=Callyl}$ from 1640 cm^{-1} in the non-coordinated SafH to ~1602 cm^{-1} in [PtCl(Saf)

Table 1
^{1}H and ^{13}C NMR signals of **1**–**4** in $CDCl_3$, δ (ppm), *J* (Hz).

Comp.	H8a	H8b	H9	H10*cis*	H10*trans*	H3	H6	Others
1 (1:1)[a]	**2.57/2.56** d ^{2}J 17 $^{3}J_{PtH}$ 105	3.79 ov	5.08 m $^{2}J_{PtH}$ 70	**4.31/4.26** d ^{3}J 7.5 $^{2}J_{PtH}$ 65	**4.0/3.98** d ^{3}J 12.5 $^{2}J_{PtH}$ 65	6.53–6.54 ov		OH: 5.31 s H7: 3.79 ov
2 (0.8:1)[a]	**2.59/2.57** d ^{2}J 16.5 $^{3}J_{PtH}$ 110	3.74–3.79 ov	5.07 m $^{2}J_{PtH}$ 70	**4.29/4.26** d ^{3}J 7.5 $^{2}J_{PtH}$ 65	4.01 d ^{3}J 13.5 $^{2}J_{PtH}$ 65	6.57 s	**6.41/6.38** S	H7a: 4.57 s H7b: 3.74–3.79 ov H11: 5.13 m H12: 1.28/1.27 t, ^{3}J 7.5
3 (1:1)[a]	2.58 d ^{2}J 16.5 $^{3}J_{PtH}$ 110	3.87−3.79 ov	5.11 m $^{2}J_{PtH}$ 70	**4.33/4.30** d ^{3}J 6.5 $^{2}J_{PtH}$ 65	4.03 d ^{3}J 13 $^{2}J_{PtH}$ 65	6.53 s	**6.47/6.46** s	H7a/H7b: 3.87−3.79 ov
4 (1:1)[a]	2.58 d ^{2}J 17 $^{3}J_{PtH}$ 110	3.79 ov	5.09 m $^{2}J_{PtH}$ 70	4.28−4.24 ov	4.01 d ^{3}J 13.5 $^{2}J_{PtH}$ 65	6.57 s	**6.43/6.40** s	H7a: 4.60 s H7b: 3.79 ov H11: 4.28−4.24 ov H12: 1.30, t, ^{3}J 7.0

Comp.	C9	C10	C1	C2	C3	C4	C5	C6	Others
2	**91.2/90.9**	**64.2/63.8**	145.4	148.7	109.2	143.6	141.1	116.9	168.7: C=O; 68.9: C11; 66.8: C7b; 56.2: C7a; 38.2: C8; 21.9: C12
3	**91.6/91.2**	**64.2/63.7**	145.2	148.1	108.4	139.4	126.0	114.0	56.0: C7a/C7b

[a] Intensitive ratio of the two sets of signals.

Table 2
^{1}H and ^{13}C NMR signals of **3**–**5** in CD_3CN, δ (ppm), *J* (Hz).

Comp.	H8a	H8b	H9	H10*cis*	H10*trans*	H3	H6	Others
3	2.65 d ^{2}J 17 $^{3}J_{PtH}$ 105	3.84−3.53 ov	5.0 m $^{2}J_{PtH}$ 70	4.14 d ^{3}J 7.5 $^{2}J_{PtH}$ 65	3.84−3.53 ov	6.47 s	6.55 s $^{3}J_{PtH}$ 42	H7a/H7b: 3.84−3.53 ov
4	2.70 d ^{2}J 17 $^{3}J_{PtH}$ 110	3.79–3.70 ov	5.01 m $^{2}J_{PtH}$ 70	4.22–4.18 ov	3.79–3.70 ov	6.68 s	6.79 s $^{3}J_{PtH}$ 42	H7a: 4.60 s H7b: 3.79–3.70 ov H11: 4.28−4.24 ov H12: 1.27 t, ^{3}J 7.5
5	2.70 d ^{2}J 17 $^{3}J_{PtH}$ 106	3.67 dd ^{3}J 17 ^{3}J 6	5.03 m $^{2}J_{PtH}$ 75	4.16 d ^{3}J 8 $^{2}J_{PtH}$ 75	3.82 d ^{3}J 13 $^{2}J_{PtH}$ 75	6.57 s	6.82 s $^{3}J_{PtH}$ 45	H7: 5.82/5.79 s

Comp.	C9	C10	C1	C2	C3	C4	C5	C6	Others
3	91.9	63.7	146.0	148.8	109.9	142.0	123.0	118.3	56.5/56.4: C7a/C7b
4	91.7	63.8	144.1	148.9	110.2	143.5	122.8	119.9	170.3: C=O; 67.0: C11; 61.8: C7a; 56.5: C7b; 39.0: C8; 14.6: C12
5	90.6	62.6	142.7	145.8	105.0	140.9	122.9	113.2	100.1: C7

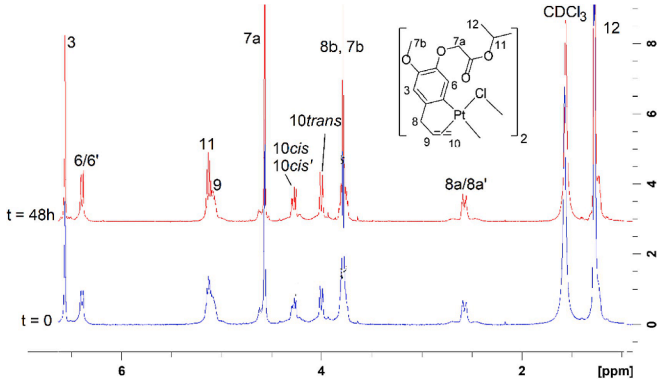

Fig. 2. The time-dependent ^{1}H NMR spectra of [Pt(*μ*-Cl)(^{i}PrEug)]$_2$ (**2**) in $CDCl_3$.

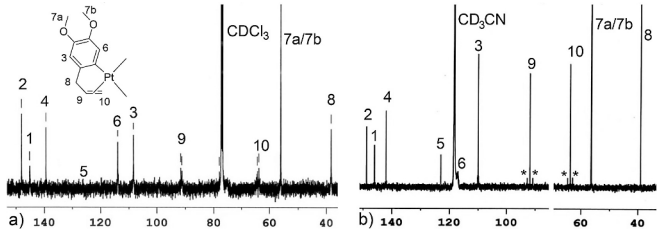

Fig. 3. (a) ^{13}C NMR spectra of **3** in $CDCl_3$ and CD_3CN (b); ^{195}Pt satellites are under the asterisks (*).

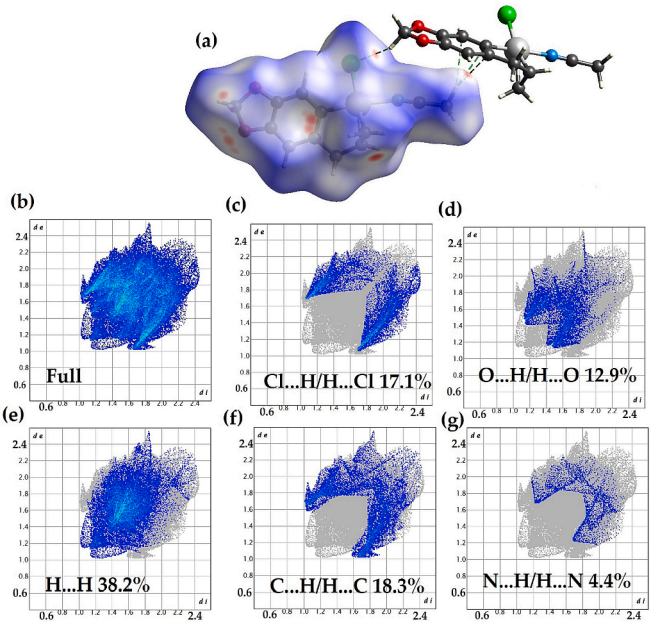

Scheme 2. The formation of *anti/syn*-[Pt(*μ*-Cl)(arylolefin)]$_2$ from K[PtCl$_3$(arylolefinH)].

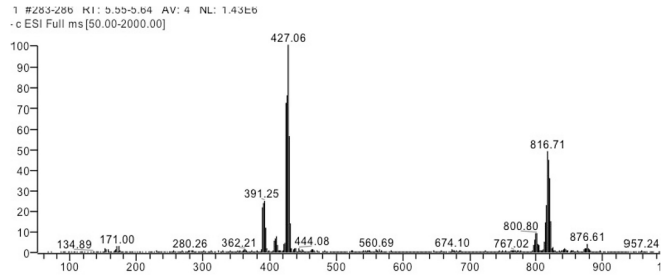

Fig. 4. ESI mass spectrum of complex [PtCl(Saf)(CD_3CN)] Fig. 4. Solid-state molecular structure of complex [PtCl(Saf)(CH_3CN)] showing 50% probability ellipsoids. Hydrogen atoms have been omitted for clarity.

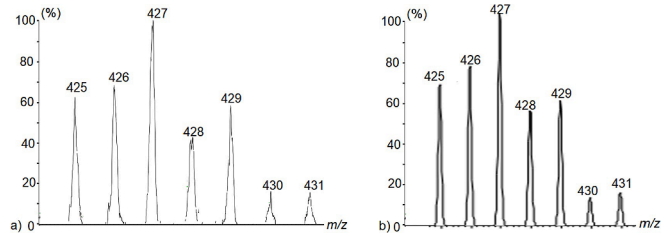

Fig. 5. (a) Experimental; (b) and simulated isotopic pattern for anion $[PtCl_2(Saf)]^-$. Fig. 5. The correlation between experimental and predicted bond distances.

(CH_3CN)] shows the coordination of Saf with Pt(II) ion *via* the C = $C_{olefinic}$ [Supporting Information Fig S15].

The single crystal X- Ray Diffraction analyses (Fig. 6) reveals that the resulting product was a monoplatinum complex [PtCl(Saf)(CH_3CN)] rather than complex **5**. The square-planar coordination environment of the Pt(II) atom is surrounded by one Cl atom, the phenyl C atom, and the C═C of the allyl group of the Saf and neutral acetonitrile. The whole crystallographic details are mentioned in Table 3 and selected bond lengths and angles are listed in Tables 4, 5. In comparison to the allyl group, CH_3CN is in the *cis* position in the structure. [PtCl(Saf)(CH_3CN)] crystallizes in the *P*2(1)/*n* space group. The observed distances for the analogues complexes [PtCl(arylolefin)(L)] (arylolefin: Saf, Eug, EtEug, ^{i}PrEug; L: monodentate amine, CH_3CN and $(CH_3)_2SO$) [16,24,26] correspond to the Pt − C9, Pt − C10, Pt − C_{aryl}, Pt − Cl, and Pt − N distances. However, it's worth mentioning that the $C_9 = C_{10}$ distance is 1.400(6) Å, which increases significantly in comparison to the non-binding Saf, 1.29(4) Å [42]. The decrease in chemical shift of the H9, H10, C9, C10 observed in the ^{1}H and ^{13}C NMR spectra support this observation.

The optimized geometries of [PtCl(Saf)(CH_3CN)] in the gas phase were obtained by combining the mixed 6-31G(d,p) and LANL2DZ basis sets with the appropriate density functional theory-based function

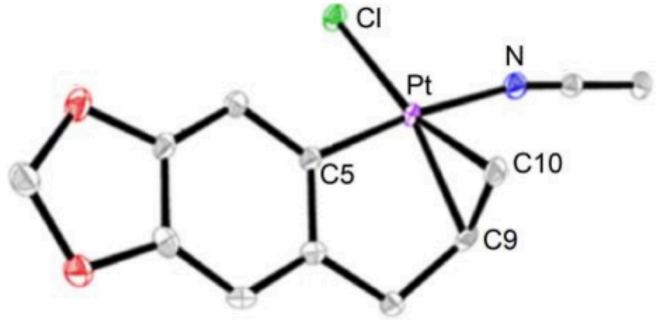

Fig. 6. (a) HOMO and LUMO plots for Pt-complex, as well as the energy gap (Egap) and (b) MEP surfaces of Pt-complex calculated by DFT study.

Table 3
Selected X-ray crystallographic data for the complex [PtCl(Saf)(CH_3CN)].

Empirical formula	$C_{12}H_{12}ClNO_2Pt$	
Formula weight	432.77	
Temperature	100(2) K	
Wavelength	0.71073 Å	
Crystal system	Monoclinic	
Space group	*P*2(1)/n	
Unit cell dimensions	a = 6.8927(11) Å	a = 90°.
	b = 10.3419(16) Å	b = 98.774 (3)°.
	c = 16.941(3) Å	g = 90°.
Volume	1193.5(3) Å^3	
Z	4	
Density (calculated)	2.408 Mg/m^3	
Absorption coefficient	11.967 mm^{-1}	
F(000)	808	
Crystal size	0.31 × 0.26 × 0.08 mm^3	
Theta range for data collection	2.43 to 27.49°.	
Index ranges	$-8\le h\le 8$, $-13\le k\le 7$, $-21\le l\le 21$	
Reflections collected	8202	
Independent reflections	2728 [R(int) = 0.0352]	
Completeness to theta = 27.49°	99.8 %	
Absorption correction	Semi-empirical from equivalents	
Max. and min. transmission	0.4477 and 0.1189	
Refinement method	Full-matrix least-squares on F^2	
Data / restraints / parameters	2728 / 0 / 159	
Goodness-of-fit on F^2	1.083	
Final R indices [I > 2sigma(I)]	R1 = 0.0249, wR2 = 0.0645	
R indices (all data)	R1 = 0.0265, wR2 = 0.0653	
Largest diff. peak and hole	2.357 and −1.604 e.Å^{-3}	

B3LYP. The computed and observed values of geometrical parameters (angles) for [PtCl(Saf)(CH_3CN)] were quite close as shown in Table 4. The correlation between experimental and predicted bond distances is R2 = 0.9977 (Fig. 5), showing that the DFT/B3LYP/LanL2DZ basis set yielded good results. The completely optimized structure of [PtCl(Saf)(CH_3CN)] was used to generate HOMO (highest molecular orbital) and LUMO (lowest molecular orbital) plots to better understand the nature of the complex using frontier molecular orbital (FMO) analysis. The resulting HOMO and LUMO energy can be utilized to figure out how complexes donate and release electrons. The energy gap of the frontier molecular orbital contributes to the structural stability of the system. FMOs also provide information on the kinetic stability and chemical reactivity of a molecule. FMOs can also be used to predict the most reactive region within a complex. The DFT calculations reveal that the HOMO and LUMO orbitals have energies of −4.99 and −1.02 eV, respectively. The energy gap of the FMO of the studied metal complex is 3.97 eV as indicated in Fig. 6a. The HOMO and LUMO energy gaps revealed that the complex under investigation has high chemical reactivity, biological activity, and polarizability. The maximum charge density was centered around the benzodioxole ring in the HOMO orbital, whereas the charge density was focused on the platinum and its neighboring atoms in the LUMO orbital, indicating that ligands involved in the formation of platinum complex can drift electrons to metal through transitions.

The physical and chemical properties of any chemical structure can be investigated using the molecular electrostatic potential (MEP) mapping (Fig. 6b). The negative and positive electron density ranged from $-6.208e^{-2}$ to $6.208e^{-2}$ a.u. The MESP is represented by the color isosurface in Fig. 6b at various points on the electron density isosurface. Red and blue in the MEP represent more electron-rich and electron-poor zones, respectively. In general, MEP plots can be utilized to understand nucleophile or electrophile attacks at more appropriate locations in chemical systems [43]. MEP mapping depicts the magnitudes of electrostatic potential in chemical systems using different colors such as green, orange, blue, red, and yellow.

Table 4
Bond lengths of [PtCl(Saf)(CH_3CN)] obtained from XRD and DFT studies.

Atom	Atom	Length/Å	Length/Å (Optimized value; DFT)	Atom	Atom	Length/Å	Length/Å (Optimized value; DFT)
Pt1	C1	1.994(4)	2.005	C1	C7	1.414(5)	1.408
Pt1	N1S	2.102(3)	2.102	C2	C3	1.374(5)	1.381
Pt1	C10	2.108(4)	2.166	C3	C5	1.376(5)	1.391
Pt1	C9	2.132(4)	2.179	C5	C6	1.372(5)	1.380
Pt1	Cl1	2.3292(10)	2.3819	C6	C7	1.399(5)	1.409

Table 5
Bond angles for [PtCl(Saf)(CH_3CN)].

Atom	Atom	Atom	Angle/	Atom	Atom	Atom	Angle/
C1	Pt1	N1S	173.59(13)	C2	C3	O1	127.8(3)
C1	Pt1	C10	86.86(15)	C5	C3	O1	110.0(3)
N1S	Pt1	C10	89.10(14)	O2	C4	O1	108.7(3)
C1	Pt1	C9	82.17(15)	C6	C5	C3	122.4(4)
N1S	Pt1	C9	91.57(14)	C6	C5	O2	127.6(3)
C10	Pt1	C9	38.57(15)	C3	C5	O2	110.0(3)
C1	Pt1	Cl1	93.76(10)	C5	C6	C7	116.7(3)
N1S	Pt1	Cl1	91.73(9)	C6	C7	C1	121.7(3)
C10	Pt1	Cl1	159.98(12)	C6	C7	C8	122.1(3)
C9	Pt1	Cl1	161.23(11)	C1	C7	C8	116.2(3)
C2	C1	C7	119.6(3)	C10	C9	Pt1	69.8(2)
C2	C1	Pt1	124.7(3)	C8	C9	Pt1	108.0(2)
C7	C1	Pt1	115.7(3)	C9	C10	Pt1	71.6(2)
C3	C2	C1	117.4(4)	C1S	N1S	Pt1	167.8(3)

The magnitude of the electrostatic potential was discovered to increase in the following order: red > orange > yellow > green > blue. The chlorine atom produced the red highlighted region of the MEP plot, which depicts the area of negative potential and may be the ideal site for electrophile attack. The highlighted blue or green area, on the other hand, emphasizes the area of positive potential and may be the optimum target for nucleophile attack. The blue and green were noticed on hydrogen atoms as well as some carbon atoms that formed electron-deficient zones. In addition, utilizing CIF of X-ray structure and Crystal Explorer (v 21.5), molecular Hirshfeld analysis and accompanying 2D fingerprint plots were generated.

Hirshfeld surfaces for [PtCl(Saf)(CH_3CN)] was mapped over d_{norm} (default parameters), displaying hydrogen bond between the chlorine atom and the hydrogen atom flanked by electronegative oxygen atoms (Fig. 7a). Another intermolecular non-bonding interaction were formed between the delocalized electrons on carbon atoms of the aromatic ring and the hydrogen atoms of another moiety of metal complex, assisting in the crystallization and production of a stable complex. Generally, the red dots on the surface represent closer contacts and negative d_{norm} values corresponding to the Cl—H and C—H… π interactions. The intermolecular interactions and their percentage distributions on the Hirshfeld surface are depicted in the 2-dimensional fingerprint plots in Fig. 7 (b-g). H…H interactions (38.2%, Fig. 7e) are a substantial contributor to the total Hirshfeld surface, while Cl…H/H…Cl (17.1% Fig. 7c), H…O/O…H (12.9%, Fig. 7d), H…C/C...H (18.3% Fig. 7f), and N...H/H...N (4.4% Fig. 7g) contacts also contribute significantly. These contributions are both substantial and significant in the crystal packing.

4. Conclusion

The results conclude that, unlike $CDCl_3$, the complexes **1**–**5** don't exist in two isomeric forms in CD_3CN; instead, the chloride-bridge is broken in CD_3CN and produce mononuclear complexes with the general formula [PtCl(arylolefin)(CD_3CN)]. In the present study, Complex **5** produce [PtCl(Saf)(CH_3CN)] complex in acetonitrile with platinum residing in the square planar environment. Furthermore, DFT studies reveal that the energy gap of the FMOs of the fully optimized mononuclear complex is 3.97 eV, suggesting that the [PtCl(Saf)(CH_3CN)] complex has strong chemical reactivity, biological activity, and polarizability. The Hirshfeld surface analysis also suggest the considerable interactions in the [PtCl(Saf)(CH_3CN)] complex.

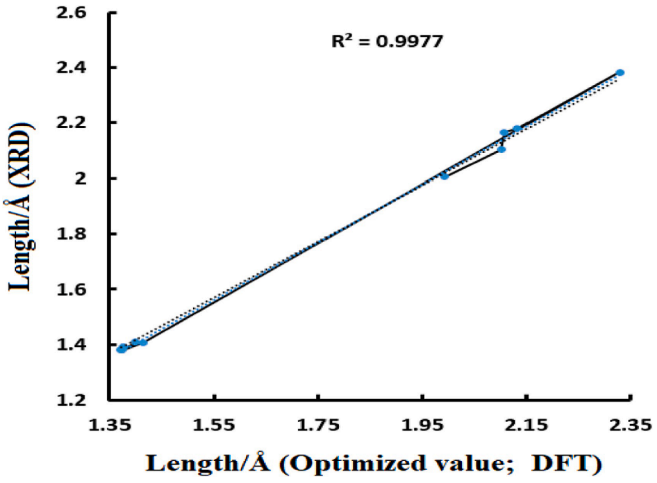

Fig. 7. (a) Hirshfeld surfaces mapped over d_{norm} with the hydrogen bond (b) [PtCl(Saf)(CH_3CN)] complex full 2D fingerprint plot (c) exhibiting reciprocal contacts and resolved into: Cl… H, (d) O… H, (e) H…H, (f) C…H, and (g) N… H showing the percentage contact contributing to the total Hirshfeld surface area of the Pt-complex.

Declaration of Competing Interest

The authors declare that they have no known competing financial interests or personal relationships that could have appeared to influence the work reported in this paper.

Acknowledgments

This research is funded by Vietnam National Foundation for Science and Technology Development (NAFOSTED) under grant number 104.03-2019.15. The authors acknowledge the financial support through Researchers Supporting Project number (RSP-2021/ 147), King Saud University, Riyadh, Saudi Arabia. The authors also thank Professor Han Vinh Huynh, Department of Chemistry, National University of Singapore for single-crystal X-ray analysis.

Appendix A. Supplementary data

CCDC 2109326 contains all data related to this paper. Supplementary data to this article can be found online at https://doi.org/10.1016/j.poly.2021.115612.

References

[1] A. Ahmedova, G. Pavlović, M. Marinov, P. Marinova, G. Momekov, K. Paradowska, S. Yordanova, S. Stoyanov, N. Vassilev, N. Stoyanov, Inorg. Chim. Acta, 528 (2021) 120605.
[2] W. Tuo, Y.L. Xu, Y.F. Fan, J. Li, M.Q. Qiu, X.X. Xiong, X.Y. Li, Y. Sun, Coord. Chem. Rev. 443 (2021), 214017.
[3] J.J. Wilson, S.J. Lippard, Chem. Rev. 114 (2014) 4470–4495.

[4] M. Azam, I. Warad, S. Al-Resayes, M. Shakir, M.F. Ullah, A. Ahmad, F.H. Sarkar, Inorg. Chem. Commun 20 (2012) 252–258.
[5] M. Azam, S. Al-Resayes, S.M. Soliman, A. Trsesowska-Kruszynska, R. Kruszynski, Z. Khan, J. Photochem. Photobiol. Biol. 176 (2017) 150–156.
[6] T.C. Johnstone, G.Y. Park, S.J. Lippard, Anticancer Res. 34 (2014) 471–476.
[7] F. Sally, F.A. John, Eur. J. Med. Chem. 37 (2002) 527–539.
[8] A. Romerosa, P. Bergamini, V. Bertolasi, A. Canella, M. Cattabriga, R. Gavioli, S. Manas, N. Mantovani, L. Pellacani, Inorg. Chem. 43 (2004) 905–913.
[9] T.T. Da, L.T.H. Hai, L.V. Meervelt, N.H. Dinh, J. Coord. Chem. 68 (2015) 3525–3536.
[10] W.C. Zeise, Ann. Phys. 97 (1831) 497–541.
[11] F.R. Hartley, Chem. Rev. 69 (1969) 799–844.
[12] U. Belluco, Organometallic and Coordination Chemistry of Platinum, Academic Press, London and New York, 1974.
[13] A. Konig, M. Bette, C. Bruhn, D. Steinborn, Eur. J. Inorg. Chem. 2012 (2012) 5881–5895.
[14] R.S. Pryadun, O.O. Gerlits, J.D. Atwood, J. Coord. Chem. 59 (2006) 85–100.
[15] T.T. Da, L.X. Chien, N.T.T. Chi, L.T.H. Hai, N.H. Dinh, J. Coord. Chem. 65 (2012) 131–142.
[16] T.T. Da, Y.M. Kim, N.T.T. Chi, L.X. Chien, N.V. Minh, N.H. Dinh, Organometallics 27 (2008) 3611–3613.
[17] M. B. Gerhard, W. S. Jeffrey. US Patent 4486179, 1984.
[18] G. Pneumatikakis, Inorg. Chim. Acta 93 (1984) 5–11.
[19] A.L. Konovalova, K.I. Yakovlev, A.I. Stetsenko, N.D. Rozhkova, G.K. Gerasimova, T. I. Ivanova, N.S. Kamaletdinov, V.P. Sinditskii, Pharm. Chem. J. 28 (1994) 21–24.
[20] T.T. Da, N.T.T. Minh, N.T.T. Chi, N.H. Dinh, Polyhedron 26 (2007) 3271–3276.
[21] T.T. Da, N.T.T. Chi, L.V. Meervelt, P.M. Kimpende, N.H. Dinh, Polyhedron 85 (2015) 104–109.
[22] L. Fang, M. Feng, F. Chen, X. Liu, H. Shen, J. Zhao, S. Gou, Bioorg. Med. Chem. 24 (2016) 4611–4619.
[23] M. Massoni, J.C. Tenorio Clavijo, L. Colina-Vegas, W. Villarreal, J.S.M. Dias, G.A. F. da Silva, M. Ionta, M. Soares, J. Ellena, A.C. Dorigueto, M.I.F. Barbosa, A. A. Batista, Polyhedron 129 (2017) 214–221.
[24] T.T. Da, Y.M. Kim, T.T.C. Mai, N.C. Cuong, N.H. Dinh, J. Coord. Chem. 63 (2010) 473.
[25] P.V. Thong, N.T.T. Chi, Vietnam J. Chem. 52 (2014) 381–386.
[26] N.T.T. Chi, T.T. Da, K. Robeyns, L.V. Meervelt, T.T.C. Mai, N.D. Dat, N.H. Dinh, Polyhedron 151 (2018) 330–337.
[27] H.V. Huynh, V.T. Pham, N.T.T. Chi, Eur. J. Inorg. Chem. 48 (2017) 5650–5655.
[28] N.T.T. Chi, V.T. Pham, H.V. Huynh, Organometallics 39 (2020) 3505–3513.
[29] M. Niazi, A. Klein, Inorganics 9 (2021) 47.
[30] S. Hizal, M. Hejl, C. Jungmann, M.A. Jakupec, M. Galanski, B.K. Keppler, Eur. J. Inorg. Chem. 2019 (2019) 856–864.
[31] Bruker, SMART (version 5.628), Bruker AXS Inc., Madison, Wisconsin, USA, 2001.
[32] Bruker, SAINT+ version 6.22a, Bruker AXS Inc., Madison, Wisconsin, USA, 2001.
[33] G.W. Sheldrick, SADABS Version 2.10, University of Göttingen, Göttingen, Germany, 2001.
[34] SHELXTL version 6.14, Bruker AXS Inc., Madison, Wisconsin, USA, 2000.
[35] Gaussian 09, Revision A.02, M. J. Frisch, G. W. Trucks, H. B. Schlegel, G. E. Scuseria, M. A. Robb, J. R. Cheeseman, G. Scalmani, V. Barone, G. A. Petersson, H. Nakatsuji, X. Li, M. Caricato, A. Marenich, J. Bloino, B. G. Janesko, R. Gomperts, B. Mennucci, H. P. Hratchian, J. V. Ortiz, A. F. Izmaylov, J. L. Sonnenberg, D. Williams-Young, F. Ding, F. Lipparini, F. Egidi, J. Goings, B. Peng, A. Petrone, T. Henderson, D. Ranasinghe, V. G. Zakrzewski, J. Gao, N. Rega, G. Zheng, W. Liang, M. Hada, M. Ehara, K. Toyota, R. Fukuda, J. Hasegawa, M. Ishida, T. Nakajima, Y. Honda, O. Kitao, H. Nakai, T. Vreven, K. Throssell, J. A. Montgomery, Jr., J. E. Peralta, F. Ogliaro, M. Bearpark, J. J. Heyd, E. Brothers, K. N. Kudin, V. N. Staroverov, T. Keith, R. Kobayashi, J. Normand, K. Raghavachari, A. Rendell, J. C. Burant, S. S. Iyengar, J. Tomasi, M. Cossi, J. M. Millam, M. Klene, C. Adamo, R. Cammi, J. W. Ochterski, R. L. Martin, K. Morokuma, O. Farkas, J. B. Foresman, and D. J. Fox, Gaussian, Inc., Wallingford CT, 2016.
[36] A.B. Nielsen, and A. J. Holder, Gauss View 5.0, User's Reference, GAUSSIAN Inc., Pittsburgh, PA, 2000–2008.
[37] P.R. Spackman, M.J. Turner, J.J. McKinnon, S.K. Wolff, D.J. Grimwood, D. Jayatilaka, M.A. Spackman, J. Appl. Cryst. 54 (2021) 1006–1011.
[38] A. König, M. Bette, C. Bruhn, D. Steinborn, Eur. J. Inorg. Chem. 35 (2012) 5881–5895.
[39] D.B. Dell'Amico, L. Labella, F. Marchetti, S. Samaritani, Dalton Trans. 41 (2012) 1389–1396.
[40] K. Praefcke, B. Bilgin, J. Pickardt, M. Borowski, Chemische Berichte 127 (1994) 1543–1545.
[41] C.N.T. Thanh, T.P. Van, H.L.T. Hong, L.V. Meervelt, Acta Cryst. C 72 (2016) 758–764.
[42] N.T.T. Chi, P.V. Thong, L.V. Meervelt, Acta Cryst. E 76 (2020) 1012–1017.
[43] S. Thijs, S. Sason Shaik, J. Am. Chem. Soc. 142 (2020) 20002-2013.